Available online at www.sciencedirect.com
ScienceDirect
Experimental Thermal and Fluid Science 31 (2007) 701–710
Experimental Thermal and Fluid Science
www.elsevier.com/locate/etfs

Identification models for transient heat transfer on a flat plate

Ali Grine, Didier Saury *, Jean-Yves Desmons, Souad Harmand

Université de Valenciennes et du Hainaut-Cambrésis, Laboratoire de Mécanique et Energétique, Le Mont Houy, 59313 Valenciennes, Cedex 9, France

Received 15 February 2006; received in revised form 21 July 2006; accepted 21 July 2006

Abstract

This paper presents new methods for identifying the convective heat transfer on a flat plate using analytical models based on the Green functions theory. The air flows over a flat plate heated by applying a controlled and transient radiative heat flux to one of its surfaces. On the opposite surface, the plate is cooled down by another air flow. The temperature profile of the plate surface is determined with an infrared camera when the plate is exposed to the controlled heat flux. Green functions are used to determine analytical solutions for the heat flux equation in the plate. These analytical solutions allow the transient convective heat transfer to be identified.

Keywords: Convective heat transfer; Transient state; Green functions

1. Introduction

Knowledge of heat transfer coefficients and their correct use is essential for optimizing the design of industrial processes involving convective heat transfer. The convective heat transfer coefficient is often estimated experimentally by coupling the wall heat flux measurement with that of the temperature of the wall over which the fluid flows. In most cases, the coefficient is determined when the steady-state thermal boundary conditions are reached [1]. In transient state experimentation with solid materials, simple thermo-kinetic models, based on the flash method [2–6] applied to a semi-infinite wall, are the most used. In most cases, using this method requires measuring the temperature and/or the heat flux on the surface subjected to thermal excitation and airflow. Such a method is not without drawbacks, however, since the thermal excitation can perturb thermal and dynamic boundary layers, as well as wall temperature and/or wall heat flux measurements.

This article proposes theoretical thermo-kinetic models to experimentally determine the heat transfer coefficient in a transient state. In steady-state conditions, this coefficient incorporates both the flow properties and thermal properties of the fluid and the wall, and is expressed by Newton's law as $\varphi = h(T_w - T_\infty)$, where h refers to the convective heat transfer coefficient. In transient-state conditions, and in the absence of complementary data, this Newton formulation tends to be extrapolated. However, in many cases, especially when boundary conditions are time dependant, this formulation appears to be inadequate, and an unsteady approach is needed.

In order to validate our theoretical models, an experimental study of the well-known flat plate exposed to a laminar airflow was carried out. The plate was heated on the surface opposite the airflow, and the instantaneous surface temperature was measured. Our objective was to develop identification models suitable for identifying the heat transfer coefficients in more complex geometries, such as the wide-ranging backward facing step, in which improving the downstream heat transfer is of paramount interest in many industrial applications.

* Corresponding author. Tel.: +33 327 511 960; fax: +33 327 511 961.
E-mail address: didier.saury@univ-valenciennes.fr (D. Saury).

0894-1777/$ - see front matter © 2006 Elsevier Inc. All rights reserved.
doi:10.1016/j.expthermflusci.2006.07.004

Nomenclature

a	thermal diffusivity (m^2/s)
e	flat plate thickness (m)
f(t)	wall temperature (°C)
G	Green function
$\overline{G}$	Laplace transform of quantity G
h_i	heat transfer coefficient on the heated surface (W/m^2 K)
h_e	heat transfer coefficient on the upper surface (W/m^2 K)
l	length m
m_0	zero-order temperature moment (K s)
S	temperature sensitivity (K/(W/m^2) or K m)
$S_{\beta i}$	reduced temperature sensitivity to $\beta_i\left(=\beta_i\frac{\partial\theta}{\partial\beta_i}\right)$ (K)
t	time (s)
T_∞	ambient temperature (°C)
T_0	initial temperature (°C)
x	space variable (m)

Greek symbols

α_n	Laplacian eigenvalues
ε	emissivity
ξ	space variable in Laplace space
$\delta(t)$	Dirac distribution
δ	spacing (m)
φ_0	heat flux density (W/m^2)
λ	thermal conductivity (W/m K)
$\theta(x,t)$	temperature difference ($=T(x,t)-T_\infty$) (K)
$\bar{\theta}$	Laplace transform of θ

Subscripts and superscripts

cv	convection
cd	conduction
e	upper
i	lower
r	radiation

Dimensionless numbers

Nu	Nusselt number
Pr	Prandtl number
Ra	Rayleigh number
S^*	normalized sensitivity $\left(=\frac{S-\min(S)}{\max(S)-\min(S)}\right)$

2. Experimental methodology and setup

2.1. Experimental methodology

One of the surfaces (lower) of a flat plate made of a homogeneous material was heated during a time t_1 using a uniform and constant radiative heat flux φ_0, while a known and imposed airflow (U, T_∞) flowed over the other side (upper) of the plate (see Fig. 1). During this time, the surface temperature of the upper face was measured. The temperature field in the plate, denoted $T(x,t)$, was assumed to be unidirectional. Using the thermo-kinetic models proposed in this paper, the heat transfer coefficient of the upper face h_e was then identified.

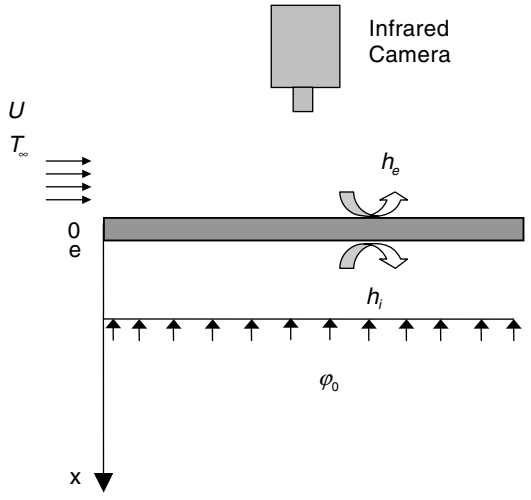

Fig. 1. Schematic presentation of the plate boundary conditions.

2.2. Experimental setup

The main element in the experimental setup [7] was a rectangular plexiglass® test section, measuring 145 mm in height, 300 mm in width and 2 m in length (see Fig. 2). A fan with a variable flow rate was used to impose the airflow. This fan was placed at the outlet of the test section in order to reduce airflow perturbation. An convergent section and a honey comb were placed at the inlet of the test section. The flat plate studied—a 4-mm thick pyrex slab measuring $170\times210\ mm^2$—was placed at the bottom of the test section as shown on Fig. 2. A set of short wavelength infrared lamps with low inertia and adjustable power was used to heat the plate. This heating system supplied a constant and controlled radiative heat flux to the flat plate. The heat flux was concentrated on the lower surface of the plate by means of an aluminium convergent section. A fluorspar (CaF_2) window was placed in front of the upper surface of the plate. Because fluorspar has a high transmission coefficient in the infrared wavelength, we were able to use infrared measurement techniques to calculate temperature. The fluorspar transmission coefficient was calibrated for the wavelength range of the IR camera (2–5.4 μm); this coefficient, equal to $\tau_f = 0.95 \pm 0.01$, remained constant.

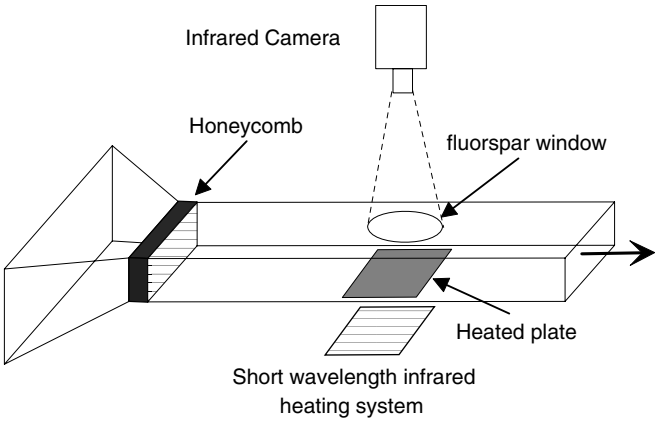

Fig. 2. Experimental Setup.

2.3. Temperature measurement

The surface temperature of the upper surface of the flat plate (over which the air flows) was determined using a short wavelength infrared camera (2–5.4 μm) equipped with a 20° lens. With an acquisition frequency of 35 Hz, this camera gives a signal $I(T)$ for a black body surface at a temperature T observed through a transparent environment. While measuring, the camera returns a digital signal from an elementary surface of the flat plate. Attenuated by the CaF_2 window and the atmosphere this signal takes the environmental radiation reflected on the plate into account [8].

The surface of the plate that was heated was painted black to increase the proportion of absorbed heat flux emitted by the short wavelength infrared lamps. The black paint also served to improve the part of radiative heat flux emitted by the plate and to increase its emissivity. This emissivity, determined by calibration, was 0.93 ± 0.02. A second calibration allowed the signal intensity $I(T)$ to be linked to the real temperature of the plate, in a real situation. Temperature uncertainty was estimated at $\Delta T = \pm 0.3$ °C for a temperature range from 30 to 100 °C. The temperature of the air in the test room was measured using two type K thermocouples, with an absolute error of about $\Delta T = \pm 0.5$ °C.

2.4. Heat flux estimation

The heat flux density was estimated through direct measurement of the radiative heat flux on the heated plate surface. Measurements were carried out with Captec radiant flux sensor. This sensor measures 10 mm wide and 300 μm thick, and has an integrated type-T thermocouple. With a response time of about 100 ms, the sensor's active elements are directly sensitive to radiative net heat flux, and thus permit the thermal flux to be balanced on the heated surface. The sensor can be used at temperatures ranging from −200 and 250 °C, and has a linear sensitivity to radiative heat flux density gauged at about 0.5 mV/(W/m^2). The relative uncertainty on the heat flux measurement depends directly on the uncertainty of the measured voltage: if S is the sensor sensibility, $\varphi = u/S$, where $\Delta\varphi/\varphi = \Delta u/u = 0.5$ %. In addition, the sensor allows temperature and radiative heat flux to be measured independently.

The sensors were calibrated at the laboratory on a specific device, but were used appropriately in other situations [9]. They were able to achieve a balance of the radiative heat flux on the irradiated surface of the plate. The relative uncertainty of the measurement remains lower than 5% for the range of heat flux variation in our experiment.

3. Analytical models for identifying h_e

In its initial state, the whole system was assumed to be at temperature T_∞. This initial temperature is used to define the temperature difference θ as $\theta(x,t) = T(x,t) - T_\infty$. The heat flux propagation in the plate was assumed to be unidirectional and to follow the law of conduction, thus,

$$\frac{1}{a}\frac{\partial\theta(x,t)}{\partial t} - \frac{\partial^2\theta(x,t)}{\partial x^2} = 0 \tag{1}$$

where the initial condition is $\theta(x,0) = 0$.

Two types of boundary conditions were investigated because they were able to provide h_e in different ways. The first type of boundary conditions assumes a constant heat transfer coefficient on both surfaces (heated and unheated). The second type assumes the temperature of the unheated face and the heat transfer coefficient of the heated face are both time dependent and known. The Green functions used to solve this problem are governed by Eq. (1) [7] and must verify

$$\frac{1}{a}\frac{\partial G}{\partial t}(x,\xi,t) - \frac{\partial^2 G}{\partial x^2}(x,\xi,t) = \delta(x-\xi)\delta(t) \tag{2}$$

with $G(x,\xi,t) = 0$ if $t \leqslant 0$ and appropriate boundary conditions (defined later on in terms of the case being investigated), the Laplace transforms of Eqs. (1) and (2) yield

$$\begin{cases} \frac{p}{a}\bar{\theta}(x,p) - \frac{1}{a}\theta(x,0) - \frac{\partial^2\bar{\theta}}{\partial x^2}(x,p) = 0 \\ \frac{p}{a}\overline{G}(x,\xi,p) - \frac{\partial^2\overline{G}}{\partial x^2}(x,\xi,p) = \delta(x-\xi) \end{cases} \tag{3}$$

Multiplying the first equation by $\overline{G}(x,\xi,p)$ and the second by $\bar{\theta}(x,p)$, Eq. (3) becomes

$$\begin{cases} \frac{p}{a}\bar{\theta}\overline{G} - \frac{1}{a}\theta(x,0)\overline{G} - \overline{G}\frac{\partial^2\bar{\theta}}{\partial x^2} = 0 \\ \frac{p}{a}\overline{G}\bar{\theta} - \bar{\theta}\frac{\partial^2\overline{G}}{\partial x^2} = \bar{\theta}\delta(x-\xi) \end{cases} \tag{4}$$

Subtracting Eq. (4) produces the following equation:

$$\frac{1}{a}\theta(x,0)\overline{G} + \left(\overline{G}\frac{\partial^2\bar{\theta}}{\partial x^2} - \bar{\theta}\frac{\partial^2\overline{G}}{\partial x^2}\right) = \bar{\theta}\delta(x-\xi) \tag{5}$$

Integrating each part of the equation over $x(0 \leqslant x \leqslant e)$,

$$\int_0^e \bar{\theta}(x,p)\delta(x-\xi)\mathrm{d}x = \int_0^e \frac{\overline{G}(x,\xi,p)}{a}\theta(x,0)\mathrm{d}x + \int_0^e \left(\overline{G}\frac{\partial^2\bar{\theta}}{\partial x^2} - \bar{\theta}\frac{\partial^2\overline{G}}{\partial x^2}\right)\mathrm{d}x \tag{6}$$

given that $\int_0^e \bar{\theta}(x,p)\delta(x-\xi)\mathrm{d}x = \bar{\theta}(\xi,p)$, and expanding the second integral into the right-hand side of Eq. (6) yields

$$\bar{\theta}(\xi,p) = \int_0^e \frac{\overline{G}(x,\xi,p)}{a}\theta(x,0)\mathrm{d}x + \begin{bmatrix} \overline{G}(e,\xi,p)\frac{\partial\bar{\theta}}{\partial x}(x,p)|_{x=e} - \bar{\theta}(e,p)\frac{\partial\overline{G}}{\partial x}(x,\xi,p)|_{x=e} \\ -\overline{G}(0,\xi,p)\frac{\partial\bar{\theta}}{\partial x}(x,p)|_{x=0} + \bar{\theta}(0,p)\frac{\partial\overline{G}}{\partial x}(x,\xi,p)|_{x} = 0 \end{bmatrix} \tag{7}$$

3.1. Identification of h_e (Model 1)

As stated above, the first model investigated assumes constant heat transfer coefficients on both surfaces (heated and unheated). This assumption will be justified at the end of this section. The boundary condition on the heated surface ($x = e$) can thus be written

$$\frac{\partial\theta}{\partial x}(x,t)|_{x=e} = -H_\mathrm{i}^0\theta(e,t) + \frac{\varphi_0}{\lambda} \tag{8}$$

where

$$H_\mathrm{i}^0 = \frac{h_\mathrm{i}^0}{\lambda} \tag{9}$$

φ_0 in Eq. (8) corresponds to the radiative heat flux density of the plate and the H_i^0 in Eq. (9) is a constant.

The boundary condition assumed for the other side of the plate ($x = 0$) is

$$\left.\frac{\partial\theta(x,t)}{\partial x}\right|_{x=0} = H_\mathrm{e}^0\theta(x,t)|_{x=0} \tag{10}$$

where $H_\mathrm{e}^0 = \frac{h_\mathrm{e}^0}{\lambda} = \frac{h_\mathrm{ec}^0 + h_\mathrm{er}^0}{\lambda}$, with h_ec^0 and h_er^0 being, respectively, the convective and radiative heat transfer coefficients, which are assumed to be constant. (This assumption will also be justified later in this paper.) The Green function solving this problem must satisfy the following boundary conditions:

$$\begin{cases} \dfrac{\partial G}{\partial x}(x,\xi,t)|_{x=0} = H_\mathrm{e}^0 G(0,\xi,t) \\ \dfrac{\partial G}{\partial x}(x,\xi,t)|_{x=e} = -H_\mathrm{i}^0 G(e,\xi,t) \end{cases} \tag{11}$$

By replacing the initial condition and the boundary conditions in (7), we obtain:

$$\bar{\theta}(x,p) = \frac{1}{\lambda}\overline{G}(e,x,p)\overline{\varphi_\mathrm{i}}(p) \tag{12}$$

The inverse Laplace transform can be used to produce the temperature profile

$$\theta(x,t) = \frac{1}{\lambda}\int_0^t \varphi_\mathrm{i}(\tau)G(e,x,t-\tau)\mathrm{d}\tau \tag{13}$$

In order to find the Green function which solves this problem, the Laplace transform of Eq. (2) is used (cf. Eq. (3), yielding

$$\overline{G}(x,\xi,p) = a\sum_{n=1}^{\infty}\frac{\psi_n(x)\psi_n(\xi)}{p + a\alpha_n^2} \tag{14}$$

where ψ_n and α_n are, respectively, the eigenfunctions and the eigenvalues of the Laplacian operator [7,10,11]. The eigenfunctions ψ_n are defined as

$$\psi_n(x) = A_n\cos(\alpha_n x) + B_n\sin(\alpha_n x) \tag{15}$$

and must satisfy the following boundary conditions for $x = 0$ and $x = e$

$$\begin{cases} \left.\dfrac{\mathrm{d}\psi_n(x)}{\mathrm{d}x}\right|_{x=0} = H_\mathrm{e}^0\psi_n(0) \\ \left.\dfrac{\mathrm{d}\psi_n(x)}{\mathrm{d}x}\right|_{x=e} = -H_\mathrm{i}^0\psi_n(e) \end{cases} \tag{16}$$

Using (15) and (16), the following transcendent equation can be obtained for the eigenvalues:

$$\tan\alpha_n e = \frac{\alpha_n(H_\mathrm{i}^0 + H_\mathrm{e}^0)}{\alpha_n^2 - H_\mathrm{i}^0 H_\mathrm{e}^0} \tag{17}$$

and for the eigenfunctions,

$$\psi_n(x) = \frac{B_n}{H_\mathrm{e}^0}\left\{\alpha_n\cos(\alpha_n x) + H_\mathrm{e}^0\sin(\alpha_n x)\right\} \tag{18}$$

Solving Eq. (17) produces an infinite number of discrete eigenvalues, and normalizing the eigenfunctions $\psi_n(x)$ $\left(\int_0^e \psi_n^2(x)\mathrm{d}x = 1\right)$ allows B_n to be determined

$$B_n^2 = \frac{2H_\mathrm{e}^{0^2}}{H_\mathrm{i}^0 + H_\mathrm{e}^0 + e(\alpha_n^2 + H_\mathrm{e}^{0^2})} \tag{19}$$

The end result is the following equation:

$$G(x,\xi,t) = a\sum_{n=1}^{\infty}\frac{B_n^2}{H_\mathrm{e}^{0^2}}\left\{\alpha_n\cos(\alpha_n x) + H_\mathrm{e}^0\sin(\alpha_n x)\right\} \times \left\{\alpha_n\cos(\alpha_n\xi) + H_\mathrm{e}^0\sin(\alpha_n\xi)\right\}e^{-a\alpha_n^2 t} \tag{20}$$

The temperature distribution $\theta(x,t)$ in the flat plate is obtained by introducing the Green function in Eq. (20) into Eq. (13), yielding

$$\theta(x,t) = \frac{\varphi_0}{\lambda}\sum_{n=1}^{\infty}\left\{\frac{B_n^2}{H_\mathrm{e}^{0^2}}\left\{\cos(\alpha_n e) + \frac{H_\mathrm{e}^0}{\alpha_n}\sin(\alpha_n e)\right\} \times \left\{\cos(\alpha_n x) + \frac{H_\mathrm{e}^0}{\alpha_n}\sin(\alpha_n x)\right\}\left(1 - e^{-a\alpha_n^2 t}\right)\right\} \tag{21}$$

$\theta(x,t)$ is continuous.

We can thus demonstrate

$$\sum_{n=1}^{\infty}\frac{B_n^2}{H_e^{02}}\left\{\cos(\alpha_n e)+\frac{H_e^0}{\alpha_n}\sin(\alpha_n e)\right\}\times\left\{\cos(\alpha_n x)+\frac{H_e^0}{\alpha_n}\sin(\alpha_n x)\right\}=\frac{\left(x+\frac{1}{H_e^0}\right)}{1+H_i^0 e+H_i^0/H_e^0} \tag{22}$$

We can also demonstrate that when t tends towards infinity, the temperature profile tends towards a limit that is not time-dependant and that corresponds to the steady state.

$$\lim_{t\to\infty}\theta(x,t)=\frac{\varphi_0/\lambda}{1+H_i^0 e+H_i^0/H_e^0}\left(x+\frac{1}{H_e^0}\right) \tag{23}$$

Please note that in steady-state conditions, the same result produced with Eq. (23) can be reproduced using thermal resistances.

This first model aims to identify the heat transfer coefficient of the upper surface of the plate without having to wait for steady-state conditions. In this model, the heat transfer coefficients of both surfaces are assumed to be constant and equal to their values in steady state.

The heat transfer coefficient is determined by comparing the experimental zero-order temperature moment and the theoretical zero-order temperature moment obtained using Eq. (21). This zero-order moment is defined as

$$m_0(x,t_f)=\int_0^{t_f}\theta(x,t)\mathrm{d}t \tag{24}$$

The time t_f, used as upper bound in this integral, is determined using the temperature sensitivity [12] to parameters such as H_e, H_i or φ_0. These reduced sensitivities are defined as

$$S_{\beta_i}=\beta_i\frac{\partial\theta}{\partial\beta_i},\quad \text{where } \beta_i=H_e,H_i \text{ or } \varphi_0 \tag{25}$$

The sensitivity values provide information about the error estimations and the possible correlations between parameters [12]. Fig. 3 plots the evolution of the reduced and normalized temperature sensitivity ($S^*_{\beta_i}=\frac{S_{\beta_i}-S^{\min}_{\beta_i}}{S^{\max}_{\beta_i}-S^{\min}_{\beta_i}}$) to H_e, H_i or φ_0 over time for different values of H_e. These quantities are evaluated using Eqs. (24) and (21). As shown in Fig. 3, the temperature sensitivity to H_e is maximum for a time equal to about 360 s, if $H_e = 13.2\ \mathrm{W/m^2\,K}$, for instance; this time value decreases as h_e increases. In addition, for the same $H_e = 13.2\ \mathrm{W/m^2\,K}$, the temperature sensitivity to H_i is maximum for a time equal to about 750 s, whereas the temperature sensitivity to φ_0 is maximum for longer time periods ($t > 1000$ s, i.e., in steady-state conditions).

According to the graphs in Fig. 3, estimating h_e is possible when the observed time remains lower than a certain value of t_f, which depends on h_e. Nevertheless, whatever the t_f value, the shortest time must be chosen. Indeed, the longer this time, the more significant the influence of h_i and φ_0. The validity of this model depends on small temperature variations in the plate to avoid significant changes in the values of the heat transfer coefficient (assumed to be constant). (This assumption will also be discussed at the end of this section.)

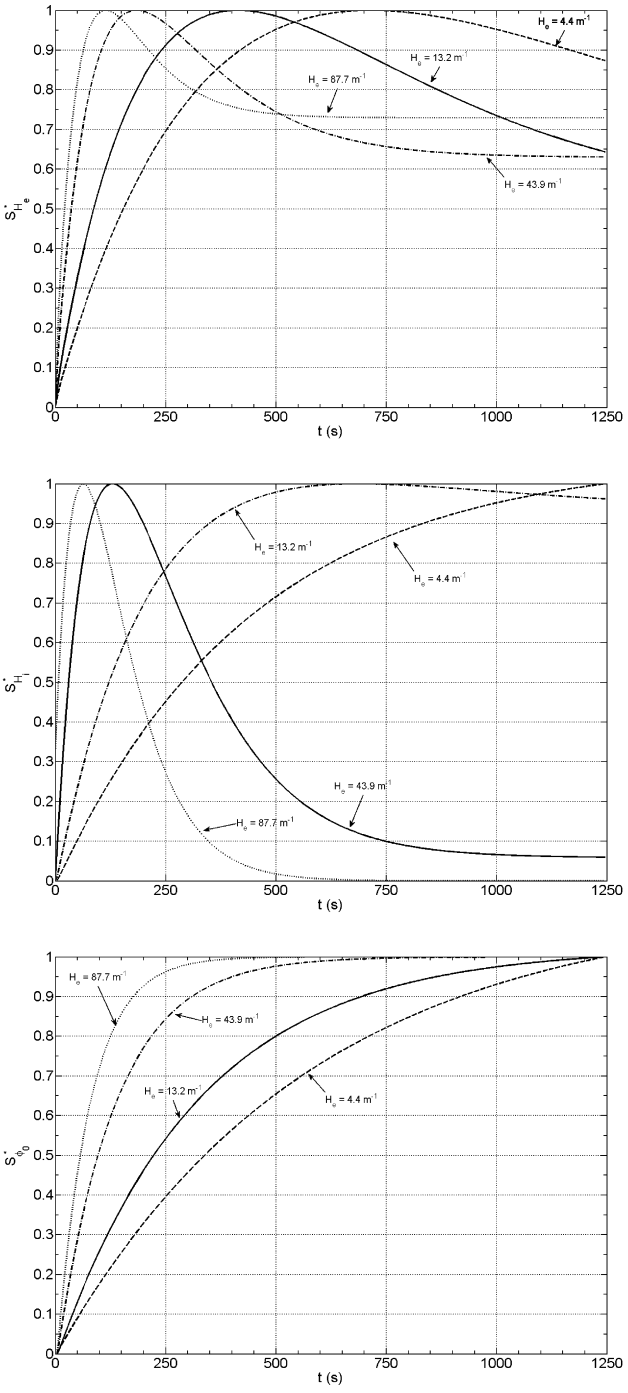

Fig. 3. Reduced temperature sensitivity to H_e, H_i and φ_0, respectively, over time for different values of H_e ($\lambda = 1.13$ W/m K).

In order to determine h_e, the coefficient's order of magnitude must be known. To do so, an iterative method can be used, starting with an arbitrary value of h_e. This value

allows the time t_f (cf. Eq. (24))—corresponding to the time when the sensitivity to h_e is maximum—to be determined. Given the temperature sensitivity to h_i, it is prudent to choose a lower value for t_f, such as $t_f/4$. This lower value insures that the temperature profile will be less dependent on H_i and φ_0 than it would be at larger t_f values. Indeed, for time $t_f/4$, the influence of H_i is lower than for larger time values (cf. Fig. 3). Thus, identifying the experimental and theoretical zero-order moment allows a new value for h_e to be determined. The iterative method presented above can be applied repeatedly until a stable value for h_e is obtained. This value corresponds to the steady-state value of h_e, obtained without having to wait for steady-state conditions since only the initial instants are considered.

The heat transfer coefficient (h_i) is not initially equal to its steady-state value, but its variation (as well as the variation of the connected heat flux density) remains low compared to the heating heat flux density. In addition, as shown in the Fig. 3, the influence of h_i on the temperature profile of the upper plate surface is initially less significant than the influence of h_e. Thus, the result is not only a consequence of the choice of h_i, but also a compromise between this choice and the sensitivity of the model to this h_i quantity (Fig. 3). In fact, the shape of the curve plotting the temperature of the upper surface is initially imposed primarily by h_e, and consequently this parameter can be identified.

Using the experimental setup described in Section 2, three different airspeeds were tested ($U_\infty = 0$ m/s, 0.5 m/s, and 1 m/s). Measurements using hot wire anemometry show that the boundary layer is a laminar flow at all 3 airspeeds. Fig. 4 depicts the early instants ($t < 150$ s) of the typical temporal evolution of the temperature difference for an airspeed of 1 m/s, measured experimentally on both surfaces of the plate. Table 1 presents the values obtained for h_e using the iterative method presented above. This table also compares the h_e values to the values obtained using model 1 (h_e^{th}) and to those obtained using literature correlations (h_e^{corr}) [13–16].

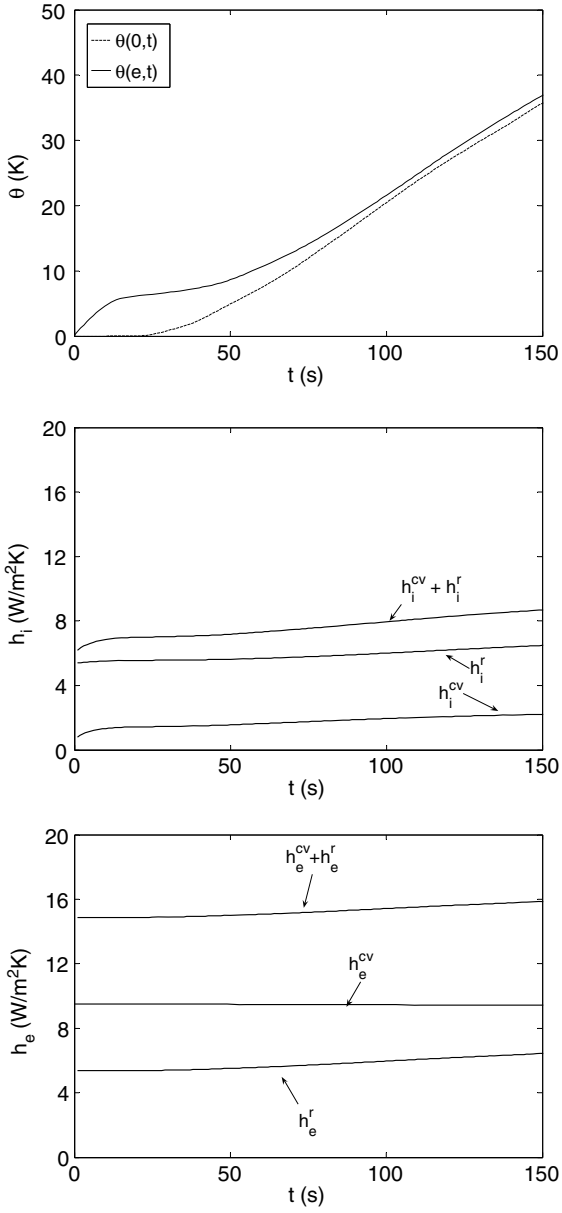

Fig. 4. Evolution of θ, h_e, and h_i over time.

- Forced convection ($Re_L < 310^5$)

$$h_e^{corr} = 0.664\frac{\lambda}{L}Re_L^{1/2}Pr^{1/3} + \frac{\varepsilon\sigma\left(T(0,\infty)^4 - T_\infty^4\right)}{T(0,\infty) - T_\infty} \quad (26)$$

- Free convection ($10^5 < Ra_L < 10^7$)

$$h_e^{corr} = 0.54\frac{\lambda}{L}Ra_L^{1/4} + \frac{\varepsilon\sigma\left(T(0,\infty)^4 - T_\infty^4\right)}{T(0,\infty) - T_\infty} \quad (27)$$

The values obtained for h_e^{th} were computed using the Nelder–Mead simplex algorithm [17], which minimizes the quadratic error between the experimental and theoretical zero-order temperature moments. These values conform to the correlations since the relative error remains lower than 3.5% in steady-state conditions, making this method appropriate for identifying the steady-state heat transfer coefficient (h_e). The originality of our method is that, regardless of the conductivity or the thickness of the plate considered, it is not necessary to wait until the system achieves a steady state to identify the heat transfer coefficient. Still, although it is true that increasing plate thickness or decreasing plate conductivity does not affect the validity of this theoretical model, it does decrease the amplitude of the external (non-heated) surface temperature, which can decrease the accuracy of the procedure. To avoid this problem, it is necessary to find a good compromise between e, λ and φ_0.

The assumption on which this first model is based is discussed below. As shown in Fig. 4, the experimental temperature variation on the lower surface of the plate is not very significant in the early instants compared to the variations

Table 1
Comparison of the values obtained for h_e using model 1 (h_e^{th}) and those obtained using correlations ($h_e^{corr} = h_e^{cv} + h_e^{r}$)

Airspeed (m/s)	h_e^{th} (W/m^2 K)	h_e^{cv} (W/m^2 K)	h_e^{r} (W/m^2 K)	h_e^{corr} (W/m^2 K)	% $h_e = \Delta h_e/h_e$
1	16.8	9.22	7.69	16.91	0.6
0.5	14.7	6.52	7.69	14.21	3.5
0	12.6	5.12	7.67	12.79	1.5

that occur later on. Fig. 4 also shows the variation of the heat transfer coefficient for the upper and lower surface of the plate obtained using experimental measurements and literature correlations [13–16]. Indeed, the variation of this coefficient ($\Delta h_i \approx 2.5$ W/m^2 K for the first 150 s) and the heat flux variation connected to this coefficient ($\Delta\varphi_i \approx 90$ W/m^2) are both negligible compared to the heat flux φ_0 used for heating (about 2500 W/m^2). The same explanation justifies the assumption made for h_e ($\Delta h_e \approx 1$ W/m^2 K and thus $\Delta\varphi_e \approx 35$ W/m^2 for the first 150 s). Indeed, during the first instants, while the temperature of lower surface of the plate is increasing, the upper plate surface temperature increases less due to the propagation time. Therefore, in the case of the first model, the assumption is justified only for the initial and the steady-state periods, and both H_e and H_i can be assumed constant.

3.2. Identification of h_e (Model 2)

Our second model assumes that the surface temperature on the non-heated surface ($x = 0$) and the heat flux density on the heated surface ($x = e$) are both known. Thus, Eqs. (1)–(7) remain valid. Only the boundary conditions change. The boundary conditions on both surfaces can now be written

$$\theta(0,t) = f(t) \quad \text{and} \quad \frac{\partial\theta}{\partial x}(e,t) = \frac{\varphi_0 - h_i\theta(e,t)}{\lambda} \tag{28}$$

The main advantage of model 2 over model 1 is that it requires no assumptions about h_e, particularly as concerns its time dependence. This second h_e identification method requires a relatively long experiment time. Unlike model 1, in which estimation is carried out for shorter times, model 2 assumes h_i to be time dependent. Thus, this second model is designed to take the time variation of h_i into account. Here, h_i can be divided into 2 parts, where the first part remains stationary (h_i^0), and the second part expresses the time variation (δh_i)

$$h_i(t) = h_i^0 + \delta h_i(t) = h_i^0 + \frac{\varsigma_i(t)}{\theta(e,t)} \tag{29}$$

The boundary conditions used for the Green function are

$$\begin{cases} G(0,\xi,t) = 0 \\ \dfrac{\partial G}{\partial x}(x,\xi,t)\big|_{x=e} = -H_i^0\, G(e,\xi,t) \end{cases} \tag{30}$$

Like in model 1, Eq. (7) (which remains valid) yields

$$\bar{\theta}(\xi,p) = \frac{1}{\lambda}\overline{G}(e,\xi,p)(\overline{\varphi_i}(p) - \overline{\varsigma_i}(p)) + \overline{f}(p)\frac{\partial\overline{G}}{\partial x}(x,\xi,p)\big|_{x=0} \tag{31}$$

The temperature of the plate is given by an inverse Laplace transform

$$\theta(x,t) = \frac{1}{\lambda}\int_0^t (\varphi_i(\tau) - \varsigma_i(\tau))G(e,x,t-\tau)\mathrm{d}\tau + \int_0^t f(\tau)\frac{\partial G}{\partial\xi}(0,x,t-\tau)\mathrm{d}\tau \tag{32}$$

By integrating Eq. (2) over x from 0 to e and using the boundary conditions, this Eq. (2) becomes

$$\frac{\partial G}{\partial x}(0,x,t) = -H_i^0 G(e,x,t) - \frac{1}{a}\int_0^e \frac{\partial G}{\partial t}(\xi,x,\tau)\mathrm{d}\xi + \delta(t) \tag{33}$$

Using this expression in Eq. (32),

$$\theta(x,t) = f(t) + \frac{1}{\lambda}\int_0^t [\varphi_i(\tau) - \varsigma_i(\tau) - h_i^0 f(\tau)] \times G(e,x,t-\tau)\mathrm{d}\tau - \frac{1}{a}\int_0^t f(\tau)\left(\int_0^e \frac{\partial G}{\partial t}(\xi,x,t-\tau)\mathrm{d}\xi\right)\mathrm{d}\tau \tag{34}$$

As in model 1, $G(x,\xi,t) = a\sum_{n=1}^{\infty}\psi_n(x)\psi_n(\xi)\exp(-a\alpha_n^2 t)$. The eigenfunctions ($\psi_n$) or eigenvalues ($\alpha_n$) must still satisfy Eq. (15). Only the boundary conditions at $x = 0$ and at $x = e$ change. Thus,

$$\begin{cases} \psi_n(0) = 0 \\ \dfrac{\mathrm{d}\psi_n}{\mathrm{d}x}(x)\Big|_{x=e} + H_i^0\psi_n(e) = 0 \end{cases} \tag{35}$$

Introducing Eq. (15) into Eq. (35) leads to both the transcendental equation for the eigenvalues α_n

$$\alpha_n\cot(\alpha_n e) = -H_i^0 \tag{36}$$

and the transcendental equation for the eigenfunctions $\psi_n(x)$

$$\psi_n(x) = B_n\sin(\alpha_n x) \tag{37}$$

Solving the transcendental Eq. (35) and normalizing the eigenfunctions $\psi_n(x)$ allows B_n to be identified

$$B_n^2 = 2\frac{\alpha_n^2 + H_i^{0^2}}{e\left(\alpha_n^2 + H_i^{0^2}\right) + H_i^0} \tag{38}$$

Finally,

$$G(x,\xi,t) = a\sum_{n=1}^{\infty} B_n^2 \sin(\alpha_n x)\sin(\alpha_n \xi)e^{-a\alpha_n^2 t} \tag{39}$$

where α_n and B_n are, respectively, the results of Eqs. (36) and (38).

The heat transfer coefficient h_e of the upper surface of the flat plate can be defined as

$$h_e = \left.\frac{\lambda\frac{\partial\theta}{\partial x}(x,t)}{\theta(x,t)}\right|_{x=0} \tag{40}$$

By defining the radiative heat flux exchange between the plate and the environment as

$$\varphi_r(0,t) = \varepsilon\sigma(T^4(0,t) - T_\infty^4), \tag{41}$$

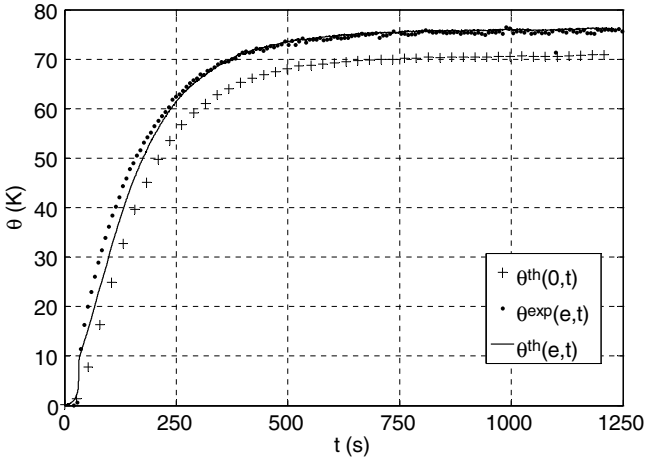

Fig. 5. Comparison between the measured and calculated temperature on the lower surface.

the convective heat transfer coefficient can be obtained

$$h_{ec}(t) = \frac{\lambda\frac{\partial\theta}{\partial x}(0,t) - \varphi_r(0,t)}{\theta(0,t)} = \frac{\lambda\frac{\partial\theta}{\partial x}(0,t) - \varepsilon\sigma(T^4(0,t) - T_\infty^4)}{\theta(0,t)} \tag{42}$$

Fig. 5 plots evolution of the temperature difference on the lower surfaces of the plate (θ_i^{th}) calculated using this second model (Eq. (34)) and the results obtained experimentally (θ_i^{exp} and θ_e^{exp}). Using the experimental boundary conditions for both surfaces, θ_i^{th} was obtained by computing Eq. (39), which provides the Green function and its partial derivative versus time. The temperature profile was obtained directly using a convolution integral between these quantities (G, h_i, f, ...). As shown in Fig. 5, the concurrence between the experimental and theoretical temperature profiles obtained is quite good. The same concurrent trend was observed in other tests carried out with other velocities (0 and 0.5 m/s). In light of these considerations, this model appears to be appropriate for analyzing the thermal behavior of a heated plate, especially for identifying the heat transfer of the non-heated surface (in this case, the upper surface, $x = 0$).

Fig. 6 presents evolution of the heat flux at $x = 0$ (φ_e, non-heated surface) and of the absorbed heat flux at $x = e$ ($\varphi_i = \varphi_0 - h_i(t)\theta(e,t)$, heated surface). This graph represents a test in which the air flows at 1 m/s over the upper surface. The same trend as for $v = 1$ m/s was observed for other velocities ($v = 0$ and $v = 0.5$ m/s). The heat flux φ_e was obtained using Eq. (34) and a forward difference at $x = 0$, thus yielding 2nd order precision. φ_i was obtained experimentally. In this figure, both the heat flux density plots have the same general trend: an initial and abrupt increase of the heat flux density up to a maximum (corresponding to about φ_0), caused by the inertia of the heating system. This increase is followed by a slight

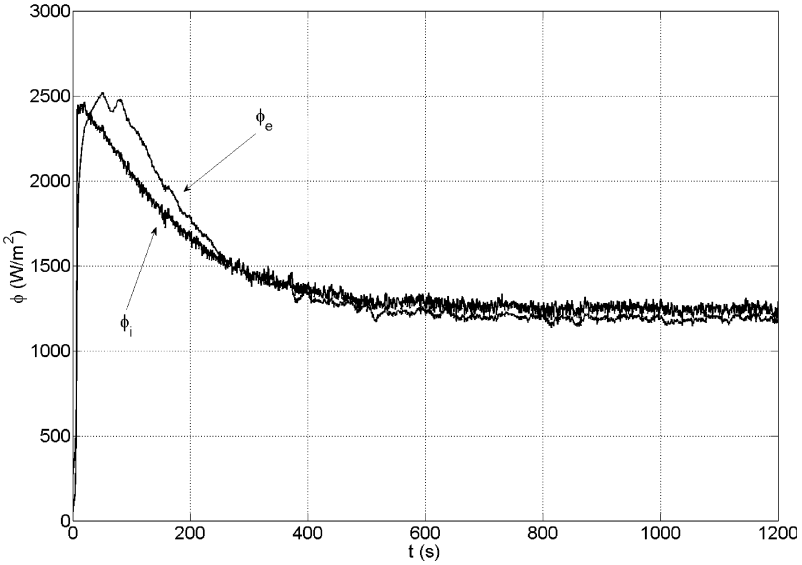

Fig. 6. Evolution of the heat flux density over time on both surfaces ($x = 0$ and $x = e$) for $v = 1$ m/s.

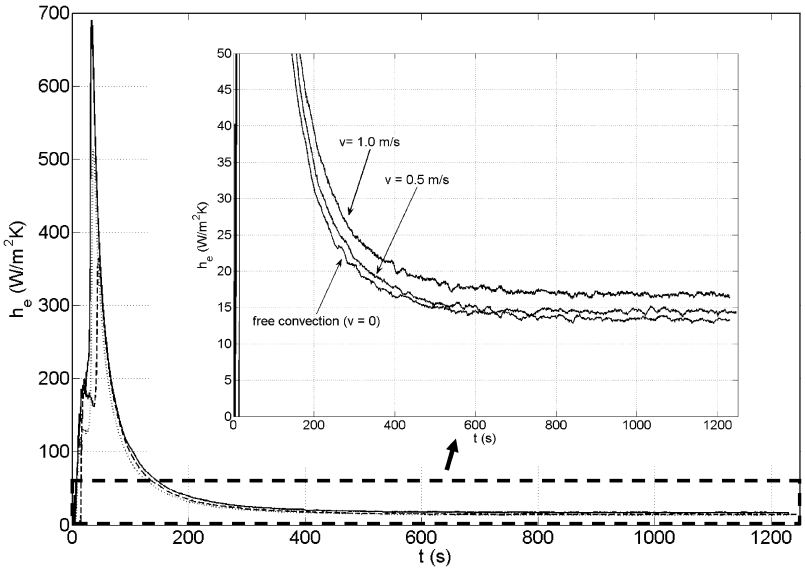

Fig. 7. Evolution of the heat transfer coefficient over time for different airflows.

Table 2
Comparison of the values obtained for h_e in steady-state conditions (h_e^{th}) using model 2 and those obtained using correlations ($h_e^{corr} = h_e^{cv} + h_e^{r}$)

Airspeed (m/s)	h_e^{th} (Model 1) (W/m^2 K)	h_e^{th} (Model 2) (W/m^2 K)	h_e^{cv} (W/m^2 K)	h_e^{r} (W/m^2 K)	h_e^{corr} (W/m^2 K)	% $h_e = \Delta h_e/h_e$
1	16.8	16.78	9.22	7.69	16.91	0.7
0.5	14.7	14.45	6.52	7.69	14.21	1.7
0	12.6	13.24	5.12	7.67	12.79	3.5

decrease due to the rise in plate temperature which promotes the radiative and convective heat transfer from the plate to the environment. For the non-heated surface, there is a delay corresponding to the propagation of this heat flux. Logically, in steady-state conditions, both the heat flux densities tend towards the same values.

Fig. 7 plots the evolution of the heat transfer coefficient on the upper surface of the plate, defined using Eq. (42). Generally, this coefficient initially increases to reach a maximum value for a very short time. Then, it decreases, tending towards a limited value corresponding to the steady-state value of h_e. This initial trend can be explained by the definition of h_e as defined in Eq. (42), which entails a singularity at time $t = 0$. Indeed, although the whole plate is initially at T_∞ (i.e., $\theta(0, t \approx 0) \approx 0$ and $T(0, t \approx 0)^4 - T_\infty^4 \approx 0$), the heat flux increases rapidly (Fig. 6). Thus, the ratio of these quantities (see Eq. (42)) has high values. As shown in Fig. 7, the three air velocities on the plate (0, 0.5 and 1 m/s) all exhibit the same decreasing trend.

The values of h_e obtained in steady-state conditions with the second model are presented in Table 2 and compared to those obtained using correlations. Like the values for the first model, these values concur since the relative error remains lower than 3.5% in steady-state conditions. In addition, unlike the first model, the second allows the time evolution of this h_e coefficient to be obtained, though this does require knowing the temperature of the non-heated surface. Still, sensitivity studies of the second model show that it is not suitable for rapid estimations of h_e since the sensitivity maximum is reached when t tends towards infinity, and the system must remain in steady-state conditions throughout the relatively long experimentation time.

4. Conclusion

This article presented two identification methods for convective heat transfer. In order to validate our models, we studied the well-known case of the flat plate with an imposed heat flux and/or temperature conditions on its surfaces. Coupled with experimental data, our models allowed us to identify the wall heat flux and the heat transfer coefficient. Green functions were used in the mathematical model employed in this identification since they allow the wall heat flux to be determined directly and rigorously, thus avoiding the need to measure the flux with the potential for disturbing the thermal boundary layer which that entails. In the first model presented, the convective heat transfer coefficient h_i^0 remains constant, which is correct in the early instants or in steady-state conditions.

This model allows the steady-state heat transfer coefficient on the non-heated surface to be identified without having to wait for steady-state conditions. The second model allows the heat transfer coefficient in transient conditions to be identified using a non-intrusive technique to determine boundary conditions. The steady-state values obtained using these two models were compared and

were found to concur. This study, which validates our identification method on a well-know case, is the first phase in a more complex project aiming to estimate the heat transfer coefficient.

References

[1] J.-F. Saccadura, Initiation aux transferts thermiques, second ed., Technique & Documentation, 1980.

[2] G. Polidori, M. Lachi, J. Padet, Unsteady convective heat transfer on a semi-infinite flat surface impulsively heated, Int. Comm. Heat. Mass. Transf. 25 (1) (1998).

[3] M. Lachi, E. Mladin, M. Rebay, J. Padet, Modélisation du couplage conduction-convection entre un écoulement et une plaque plane, Congrès SFT 2002, Vittel, 3–6 juin , 2002, pp. 101–106.

[4] D.J. Crowther, J. Padet, Measurement of the local convection coefficient by pulsed photothermal radiometry, Int. Heat Mass Transf. 34 (12) (1991) 3075–3081.

[5] R.C.C. Wang, B.T.F. Chung, L.C. Thomas, Transient convective heat transfer for laminar boundary layer flow with effect of wall capacitance and resistance, Heat transf. 99 (1977) 513–519.

[6] G. Maranzana, S. Didierjean, B. Rémy, D. Maillet, Experimental estimation of the transient free convection heat transfer coefficient on a vertical flat plate in air, Int. Heat Mass Transf. 45 (2002) 3413–3427.

[7] A. Grine, J.-Y. Desmons, S. Harmand, Models for transient conduction in a flat plate subjected to a variable heat flux, Appl. Therm. Eng., in press, doi:10.1016/j.applthermaleng.2006.06.013.

[8] F. Boizumault, S. Harmand, B. Desmet, Convective heat transfer inside a rotating cylinder with an axial air flow, Quantitative Infrared Thermography QIRT'96, Stuttgart, Germany, September 2–5, 1996, pp. 141–146.

[9] S. Seghir-Ouali, D. Saury, S. Harmand, O. Phillipart, D. Laloy, Convective heat transfer inside a rotating cylinder with an axial air flow, Int. J. Therm. Sci., in press, doi:10.1016/j.ijthermalsci.2006.01.017.

[10] D. Khaine, J.Y. Desmons, R. Ben Younés, M. Le Ray, Simulation du comportement thermique d'un local par la méthode des fonctions de Green, Int. J. Therm. Sci. 38 (1999) 340–347.

[11] A. Grine, J.Y. Desmons, S. Harmand, Modélisation des échanges convectifs en régime transitoires sur plaque plane, Congrés SFT 2005, Reims, 30 mai–2 juin, 2005, pp. 331–336.

[12] B. Remy, A. Degiovanni, Parameters estimation and measurement of thermophysical properties of liquids, Int. J. Heat Mass Transf. 48 (2005) 4103–4120.

[13] M.M. Yovanovich, K. Jafarpur, Bound on laminar natural convection from isothermal disks and finite plates of arbitrary shape for all orientations and Prandtl numbers, ASME Winter Annual Meeting, HTD-Vol. 264, New Orleans, Louisiana, November 28–December 3, 1993, pp. 93–111.

[14] M. Fishenden, O.A. Saunders, An introduction to heat transfer, Oxford University Press, London, England, 1950.

[15] W.H. McAdams, Heat transmission, third ed., McGraw-Hill Compagnies, New-York, USA, 1954.

[16] M.M. Yavanovich, General expression for laminar forced and natural convection heat transfer from isothermal flat plates for all Prandtl numbers, AIAA 28th Thermophysics Conference, Orlando, Florida USA, July 6–9, 1993, pp. 1–6.

[17] J.C. Lagarias, J.A. Reeds, M.H. Wright, P.E. Wright, Convergence properties of the Nelder–Mead simplex method in low dimensions, SIAM J. Optim. 9 (1) (1998) 112–147.